IEEE Access
Multidisciplinary | Rapid Review | Open Access Journal

Received August 28, 2020, accepted September 22, 2020, date of publication September 28, 2020, date of current version October 7, 2020.

Digital Object Identifier 10.1109/ACCESS.2020.3027154

Measurement of Potato Volume With Laser Triangulation and Three-Dimensional Reconstruction

ZEYU CAI[1], CHENGQIAN JIN[1], JING XU[2], AND TENGXIANG YANG[1]
[1]Ministry of Agriculture and Rural Affairs, Nanjing Institute of Agricultural Mechanization, Nanjing 210000, China
[2]Jiangsu Institute of Metrology, Nanjing 210000, China

Corresponding author: Chengqian Jin (jinchengqian@caas.cn)

This work was supported in part by the Special Fund Project for the Construction of Modern Agricultural Industrial Technology Systems under Grant CARS-04-PS26, in part by Jiangsu University, and in part by the Jiangsu Collaborative Innovation Center for Modern Agricultural Equipment and Technology under Grant 4091600010.

ABSTRACT Potato grading is related to weight. Three-dimensional (3D) reconstruction can provide highly accurate volume measurements of potatoes, which can help farmers to analyze their phenotypic characteristics and grade them. Considering their low cost and the required accuracy, a monocular camera and line laser were used to build a potato phenotype determination scanning device. The system obtains coordinates along the surface of a potato, collects laser light reflected from the surface in real time, and completes the coordinate calculation of the original points using the triangulation method. However, the original point clouds lose large areas of point clouds at the top and bottom of the potato. Point cloud repair is carried out by interpolation of points. In addition, the surface point cloud is smoothed. Finally, the generated point cloud is used for 3D reconstruction and volume calculation. In a volume error analysis test, potatoes are divided into calibration and verification groups. First, linear regression is used to relate the real and measured potato volume, and then the density of the potato is calculated. The volume and mass of potatoes in the verification group are measured by the device, and the standard volume and mass are measured manually. The results show that the average relative error in measured volume is −0.08%, and the average relative error in estimated mass is 0.48%. These results indicate that the combination of a line laser and a single camera provides accurate measurements of potato volume that can be used for yield estimation and potato grading.

INDEX TERMS Line laser, volume estimation, feature prediction, weight estimation.

I. INTRODUCTION

Non-destructive measurement methods are important for yield monitoring. Mechanical sensors, such as belt weights and impact measurements, can damage crops and are difficult to calibrate due to vibration. By measuring the volume of cultivated crops or agricultural products, yields can be accurately calculated [1], [2]. Geometric characteristics and yield monitoring of crops can give farmers feedback [3] that can help them grade fruits and vegetables for added value [4], [5]. However, the analysis of phenotypic features is mostly artificial [6], which is labor-intensive and inefficient, resulting in a so-called ''phenotyping bottleneck'' [7], [8]. Using computer vision [9] or three-dimensional (3D) imaging [10], farmers can analyze the quality of crops, so they can estimate yields and grades [11].

The potato (Solanum tuberosum L.) is one of the most important crops around the world, totaling 17.6 million hectares (FAO, 2018). In many cases, it is difficult to measure and grade potatoes due to their uneven surface and vulnerability to damage [12]. In the last decade, with the development of machine vision, images have been widely used to analyze the quality and weight of fruits and vegetables [13]–[15], including potatoes [16], [17]. However, the thickness of the potato cannot be obtained without the depth of field in a two-dimensional image. 3D reconstruction technology allows for precise measurements of potato volume [18], and phenotypic reconstruction has become possible.

The associate editor coordinating the review of this manuscript and approving it for publication was Chao Tan.

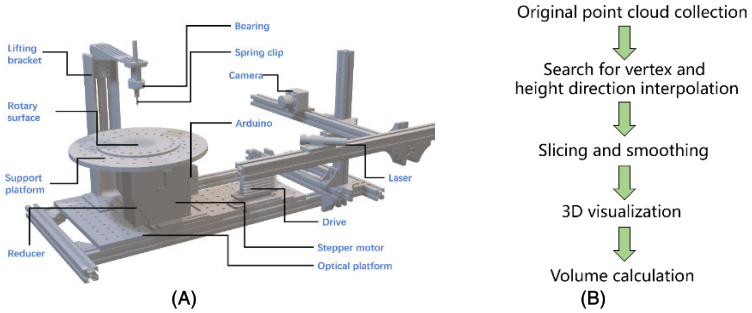

FIGURE 1. (A) Device structure. (B) Reconstruction process.

3D reconstruction has long been used to measure forest canopy parameters [19]–[21] and to monitor crop phenotypes [22], [23] and poultry [24]–[26]. It also has been used to measure the volume of crops, such as the fresh weight of lettuce [27], volume of onion fruit [28], or volume of cauliflower [29]. 3D laser scanning provides fast measurements with moderate accuracy and low cost [30]. Common methods include the use of structured light [31], [32] and time-of-flight measurements using the phase of received light [33], where the former is most used in 3D modeling, such as with the Microsoft Kinect sensor. However, due to the complexity of crop phenotypes, it is difficult to complete scanning from one angle at a time. There have been studies using multi-view stereovision [34]–[36] and structure from motion [37]–[39].

This study aims to use a single camera and line laser to build a 3D reconstruction system for potato volume measurements, through which potato surface information can be collected and stored. By analyzing point cloud data, the appearance of a potato can be reconstructed, and the exact volume calculated. Due to the limitations of a low-cost device and the influence of the camera angle, the camera cannot move and collect color information from the surface, resulting in point cloud measurements with missing information, especially at the bottom and top of a potato's rotation axis. To remedy this problem, we process the original point cloud data and reconstruct a 3D model of the potato from a grid. The potato volume measurement error from the device is determined by comparing the exact volume to the standard volume container. A non-destructive method is used to predict the weight of potatoes.

II. MATERIALS AND METHODS

A. POTATO SAMPLES AND MANUAL ASSESSMENT

The sampling standard refers to GB/T 8855-2008, and the minimum sampling quantity is 3 kg. Fresh potatoes were purchased in the afternoon from Qixia Agricultural Market of Nanjing on the day before the experiment. The total weight of 35 fresh potatoes was 6.056 kg; potatoes were randomly selected and did not have deformities. All potatoes were manually cleaned and washed to remove dirt and clay clouds before testing. The potatoes were separated into groups for calibration and verification. The weight of five potatoes used for calibration was 0.835 kg, and the weight of 30 potatoes used for verification was 5.221 kg.

The volume of potatoes was measured manually by a metrologist at Jiangsu Institute of Metrology at a constant temperature of 20°C and 50% RH. The standard device used for volume measurement is a standard glass gauge, which has an error of −0.07% in 500 mL. An electronic counting balance (Sartorius, Germany) with an error of 0.04% within 1000 g was used for mass measurement.

B. HARDWARE AND SYSTEMS

The hardware system is shown in Fig. 1A. The motion mechanism is composed of a reducer with a deceleration ratio of 2.5:1, a stepping motor (57 steps, SNOWIT, Changzhou), a two-phase DC synchronous subdivision step driver (LiChuan, Shenzhen), and an Arduino UNO R3 microcontroller board (Arduino, Italy). The data acquisition system consists of a 532-nm linear laser with 10 mW output power, and a 2048 × 1536 pixel CCD camera with a focal length of 21 mm. The system is controlled by a computer (Intel i5 CPU, Windows 7 operating system, 16 GB RAM, Hewlett Packard, USA). Both the camera and laser were placed 300 mm from the rotation axis, and the angle between the camera and laser was set to 50°.

A program for controlling the system was written in LabVIEW 2019 SP1 (National Instruments, USA); the data acquisition process is shown in Fig. 1B. Access 2016 (Microsoft, USA) was used for data storage, and MATLAB R2019a (MathWorks, USA) for 3D visualization.

C. ORIGINAL POINT CLOUD COLLECTION

A flowchart of the process for acquiring original point cloud coordinates is shown in Fig. 2A. The potato is placed on a rotating surface, and the compression force of a spring clip is used to fix the potato to the surface. The stepping motor drives the reducer and rotates the surface. Data are gathered by rotating the potato 1° in 0.5 s.

The camera is used to gather successive images as the motor moves through each step. The coordinates of points on the potato surface are calculated by image processing. A schematic diagram is shown in Fig. 2B. The actual radius r of the potato surface point and the imaging distance Δd in the image are related by the formula

$$\frac{\mathrm{r}\cdot sin\gamma}{\Delta d\cdot sin\beta} = \frac{f-\mathrm{r}\cdot cos\gamma}{f'+\Delta d\cdot cos\beta} \tag{1}$$

where r is the distance to the center of rotation for the potato surface point; Δd is the distance between the light contour

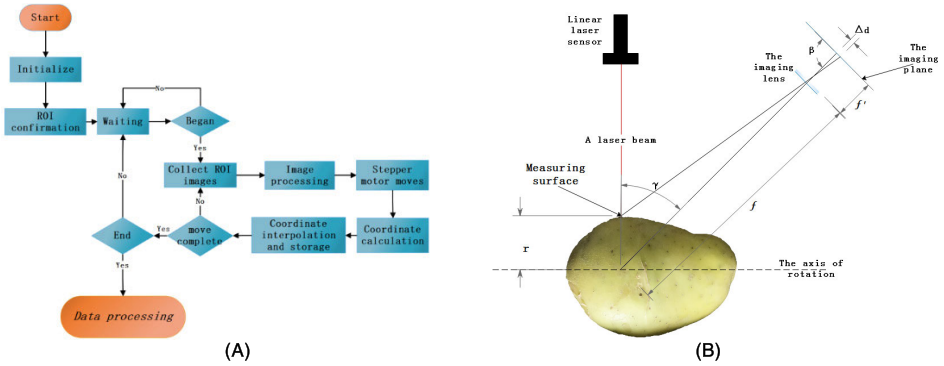

FIGURE 2. (A) Flowchart of the process for acquiring original point cloud coordinates. (B) Schematic diagram of radius coordinate calculation.

and the axis of rotation on the imaging surface; γ is the angle between the laser beam axis and the optical axis of the imaging lens; β is the angle between the imaging surface and the optical axis of the imaging lens; f is the object distance on the optical axis of the imaging lens; and f' is the image distance on the optical axis of the imaging lens. The missing point coordinates in the original coordinate data are interpolated, and all coordinates are stored in the database. The ratio of the pixel coordinates of the ROI area in the image to the actual coordinates is stored in the computer memory, and the ROI area is determined manually. Images collected by the camera are converted to 32-bit RGB format. The green component in the image is converted to an 8-bit grayscale image, which is transformed to a matrix. The program traverses each column of the matrix, calculates its brightness value using a threshold method [40], [41], and coordinates of the laser centerline in the picture are obtained. The centerline coordinates of the potato contour are compared to the axis coordinates to obtain the coordinates of the points at θi. A small number of noise points in the point cloud cause the centerline to be discontinuous. These isolated points can be removed by threshold judgment. Cubic interpolation is carried out to make discontinuous coordinate points continuous within the original range, and all coordinates are stored in an Access database. This process is repeated until the potato has rotated through a full revolution.

D. SEARCH FOR VERTEX AND HEIGHT DIRECTION INTERPOLATION

In the process of collecting the original point cloud coordinates, a large region of data will be missing from the bottom and top of the potato due to the camera angle, occlusion of the fixed device, and self-occlusion of the potato, as shown in Fig. 3A. Methods to repair 3D point clouds include implicit surface reconstruction with radial basis functions [42], surface hole filling with a context sampling model [43], and point cloud repair using Poisson's equation [44] or partial differential equations [45]. These methods are computationally intensive and may lose some detail. This study is based on the original data-acquisition device in potato fixation. There are two fixed points along the Z-axis direction, so all points in the missing area will intersect at one point. Finally, the missing points can be repaired by interpolating the intersection point and the point at each angle.

In the program, the missing regions of the point cloud at the top and bottom of the potato are first extracted, and points from 15 layers outside the missing regions are taken as the interpolation regions, as shown in Fig. 3B. The top and bottom interpolation regions are searched to find the point closest to the Z-axis and the point with the lowest height at the bottom. Points on the angles of the two search points are fitted to obtain the points intersecting the Z-axis, as shown in Fig. 3C. Various angles on the potato are traversed, and the coordinates of all the points at each angle are interpolated to obtain filled point cloud coordinates. The repaired point cloud is shown in Fig. 3D.

E. SLICING AND SMOOTHING

Point clouds on the surfaces of potatoes can be divided into two categories. The first contains unprocessed raw data, and the second contains data obtained through interpolation. Each layer is sliced according to the Z-axis, and one finds that coordinate points with no interpolation in the cross section are smooth in polar and x-y coordinates, as shown in Fig. 4A. The coordinates of the points on the interpolated cross section are too scattered, as shown in Fig. 5A. To reduce variance in the interpolation region of the point cloud, the data are fitted to a B-spline curve, which is often used for modeling in mechanical 3D design software [46], to obtain a smooth contour. All points on each slice are fitted to B-spline curves to obtain a smooth contour, as shown in Figs. 4B and 5B. By controlling the RMSE threshold of the distance between the original point and the B-spline curve, a small fluctuation is obtained and superimposed on the B-spline fitting curve. The optimized point cloud coordinates are shown in Figs. 4C and 5C.

F. VOLUME CALCULATION

The volume of the potato is calculated using the point cloud in cylindrical coordinates, as shown in Fig. 6A. The system reads all point cloud coordinates from the Access database, with coordinates formatted as shown in eq. (2). The area of the slice at height $h^j_{\theta_i}$ is integrated, as shown in eq. (3). Finally, the total volume of potatoes can be obtained by integrating the

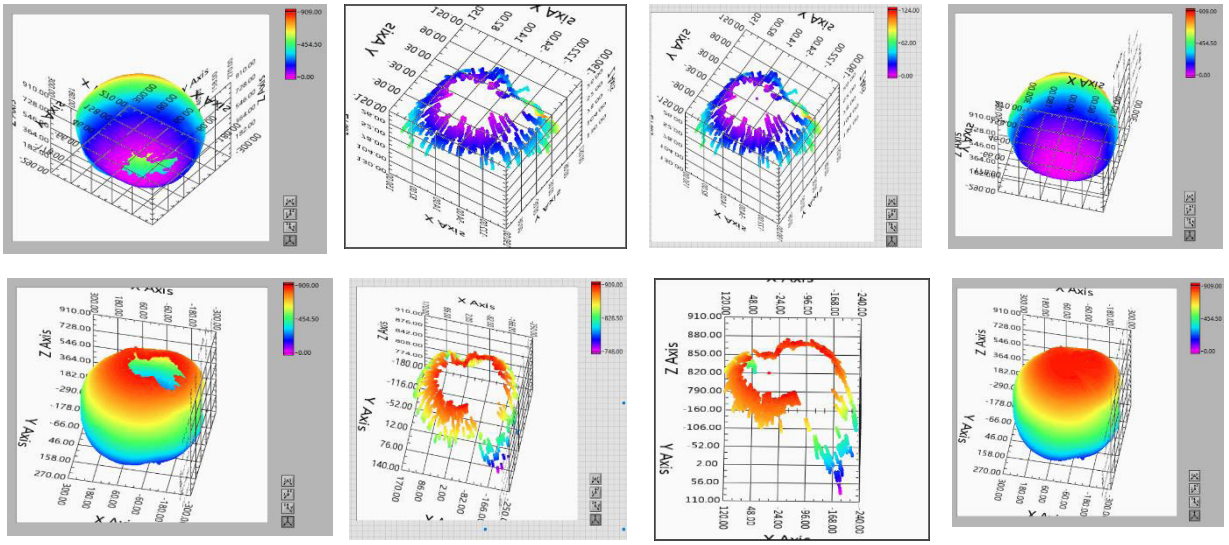

FIGURE 3. Point cloud interpolation process. (1) Point cloud from the bottom of a potato. (2) Point cloud from the top of a potato. (A) Original point cloud. (B) Point cloud interpolation region. (C) Region used to search for the intersection point. (D) Repaired point cloud.

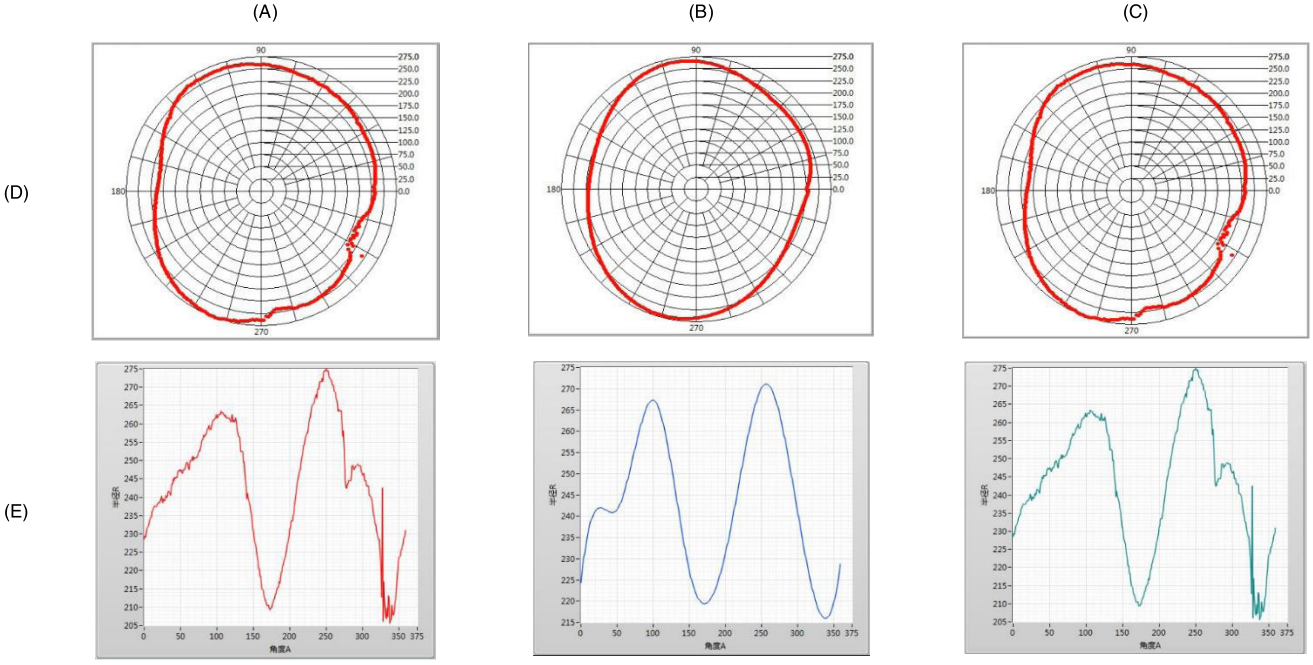

FIGURE 4. Slice graph of a point cloud region without interpolation. (A) Original point cloud. (B) B-spline fitting curve. (C) Processed point cloud in: (D) polar coordinates; and (E) Cartesian coordinates.

height of area S^j, as shown in eq. (4):

$$\vec{P}^j_{\theta_i} = \left(\theta_i, h^j_{\theta_i}, r^j_{\theta_i}\right) \tag{2}$$

$$S^j = \sum_0^n \frac{\Delta\theta_i \cdot \pi \cdot \left(r^j_{\theta_i}\right)^2}{360} \tag{3}$$

$$V = \sum_0^m \left(\sum_0^n \frac{\Delta\theta_i \cdot \pi \cdot \left(r^j_{\theta_i}\right)^2}{360} \right) \cdot \Delta h^j. \tag{4}$$

$\theta^j_{\theta_i}, h^j_{\theta_i}, r^j_{\theta_i}$ are respectively the measurement angle, height, and radius of the surface point in cylindrical coordinates; S^j is the area of the section corresponding to height Δh^j at height $h^j_{\theta_i}$; $\Delta\theta_i$ is the stepping angle; n is the number of measurement angles; and m is the total number of potato slices along the Z-axis.

III. RESULTS

A. SYSTEM CALIBRATION RESULTS

The potatoes used for calibration were measured, and the measured volume, standard volume, and standard mass were determined. Relationships between the measured volume and standard volume, and between the standard volume and standard mass, were determined using linear regression, as shown in Figs. 7A and B, respectively.

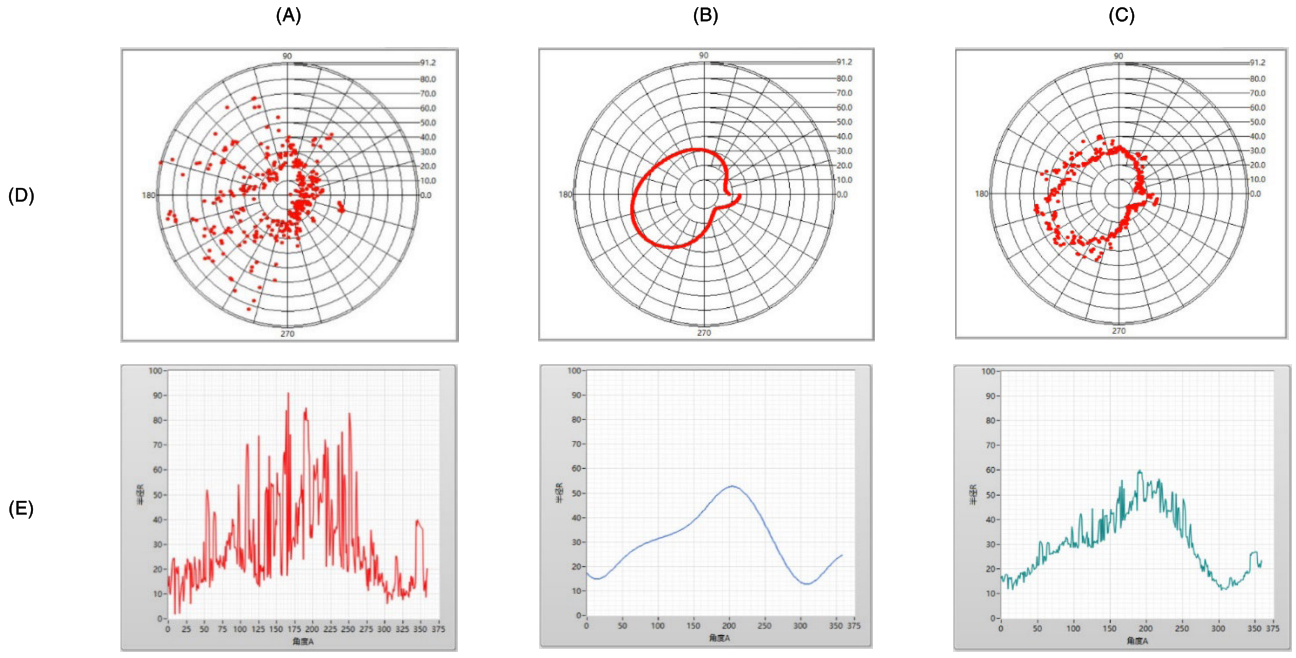

FIGURE 5. Slice graph of a point cloud region with interpolation. (A) Original point cloud. (B) B-spline fitting curve. (C) Processed point cloud in: (D) polar coordinates; and (E) Cartesian coordinates.

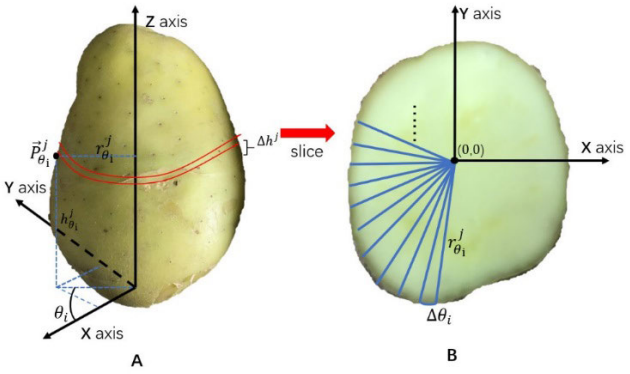

FIGURE 6. Potato volume calculation results. (A) Potatoes in Cartesian and cylindrical coordinates. (B) Potato slice area integration region.

SPSS version 23.0 (IBM Corp., Armonk, NY, USA) was used to perform linear regression between the measured volume and standard volume; the resulting model is shown in eq. (5):

$$V = V_0 * 0.992 + 13.171, \tag{5}$$

where V is the corrected volume and V_0 is the measured volume. The coefficient of determination is 1.000 and RMSE = 1.02 cm^3. The average density of potatoes used for calibration was calculated to be 1.0805 g/cm^3.

B. VERIFICATION OF POTATO VOLUME

For the point cloud used for verification, the volume was calculated using eq. (3), and the volume and mass were determined using eq. (4) and the potato density. The standard volume and standard mass were measured manually, as shown in Fig. 8.

C. CHANGE OF POTATO VOLUME DURING ALGORITHM PROCESSING

In processing the potato point cloud, the steps to change the computational value of potato volume include interpolation and smoothing. The volume of a potato is obtained in two processing steps. The volumes of the unprocessed potato point cloud, interpolated potato, and smooth potato are shown in Figure 9.

D. 3D RECONSTRUCTION

3D reconstruction of potatoes was accomplished using the alphaShape [47] toolbox in MATLAB. The surface mesh effect of the potato based on the original point cloud and the treated post-point cloud is shown in Figs. 10A–C. The maximum alpha radii of the original and processed point clouds are respectively 12 and 3 mm. For the potato in the figure, the relative error between the original point cloud volume and the standard volume is −2.12%, and the relative error between the treated point cloud volume and the standard volume is −0.98%, where the uncertainty of the standard volume measurement is 0.96%.

We materialized the surface mesh of the potato using Geomagic Wrap 2017 (3D Systems, USA) and printed a materialized model using a 3D printer with a precision of 0.2 mm from polylactic acid material. The models of real potatoes and 3D printed potatoes are shown in Figs. 11A–C.

IV. DISCUSSION

A fixed wire laser and camera were used to complete a full revolution surface scan by rotating a potato. The device can also be used to measure the volumes of vegetables and fruits, such as sweet potatoes, corn, oranges, and avocados. However, this device is not suitable for apples, pears, and

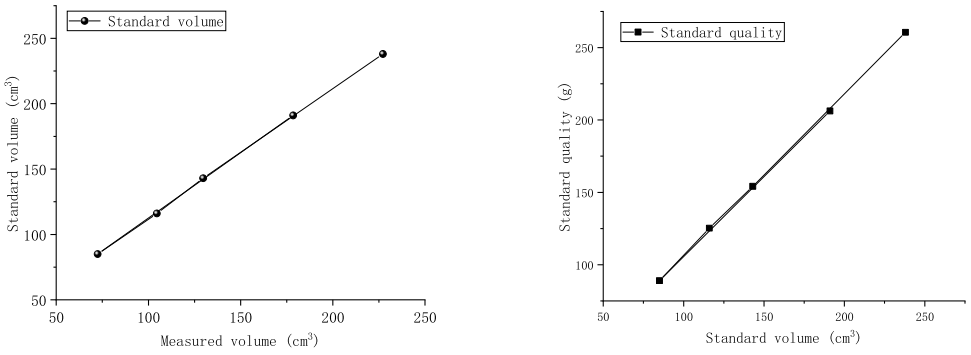

FIGURE 7. Linear regression results between: (A) measured volume and standard volume; and (B) standard volume and standard mass.

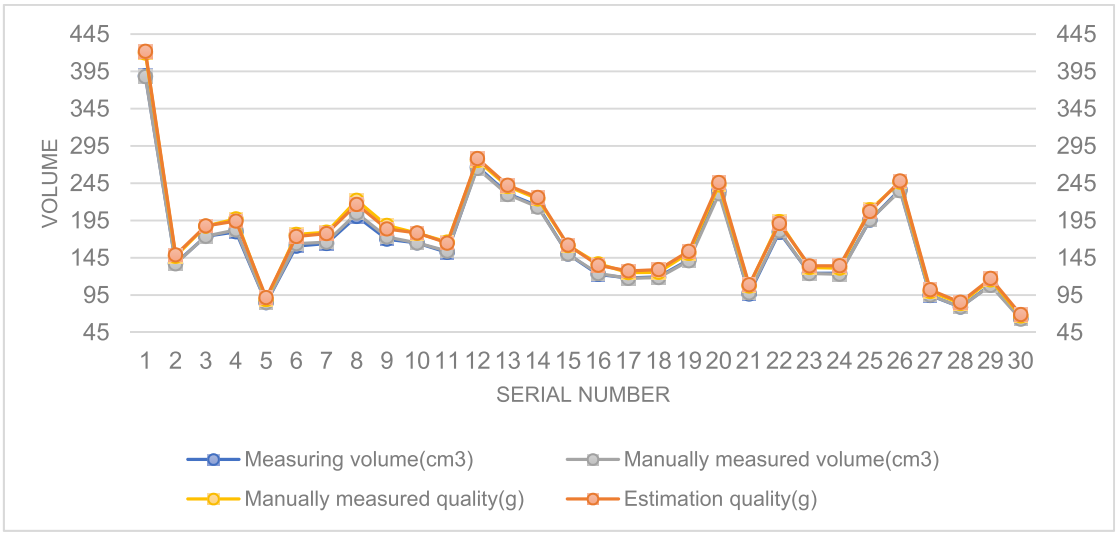

FIGURE 8. Volume and mass measurements.

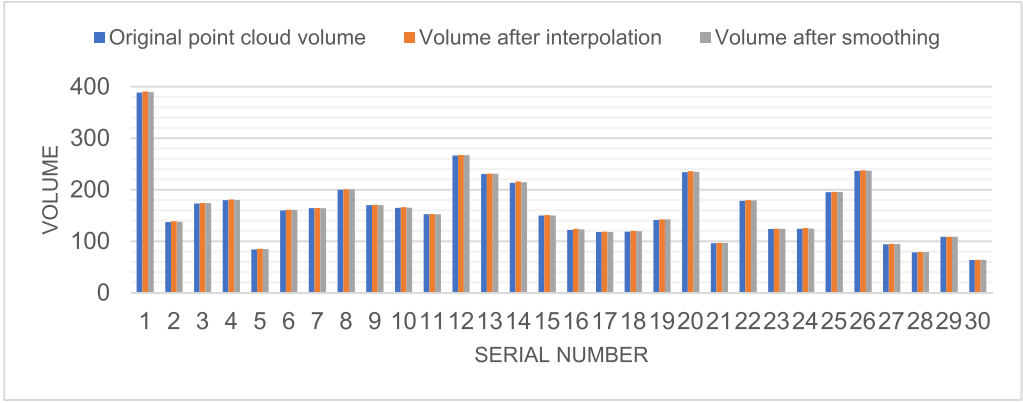

FIGURE 9. Potato volume change during point cloud processing.

other fruits with large depressions at the top, which cause large distortions in the local area. This can be solved by gathering data from multiple azimuths or by using a point cloud registration method [48], [49].

Local vertex search, interpolation, slicing, and smoothing are used in data processing to improve the detail effect of the 3D model, reducing the alpha radius after point cloud processing from 12 to 3 mm. The relative error of volume measurement after different processing steps of potatoes is shown in Fig. 12.

From the relative error of potato volume after different treatments, the calculated average relative error of the original

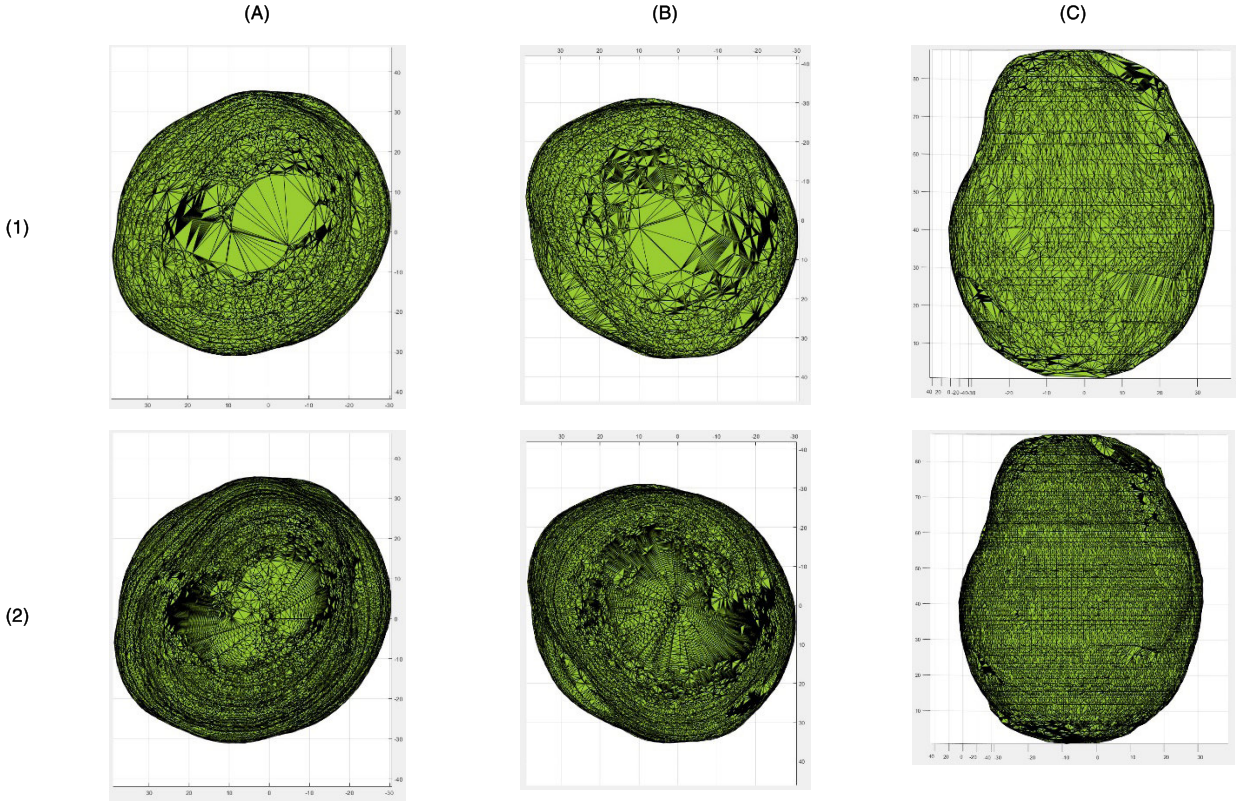

FIGURE 10. Point clouds of potatoes. (1) Grid diagram of an original point cloud. (2) Grid diagram of a processed point cloud. (A) Top of a potato. (B) Bottom of a potato. (C) Side of a potato.

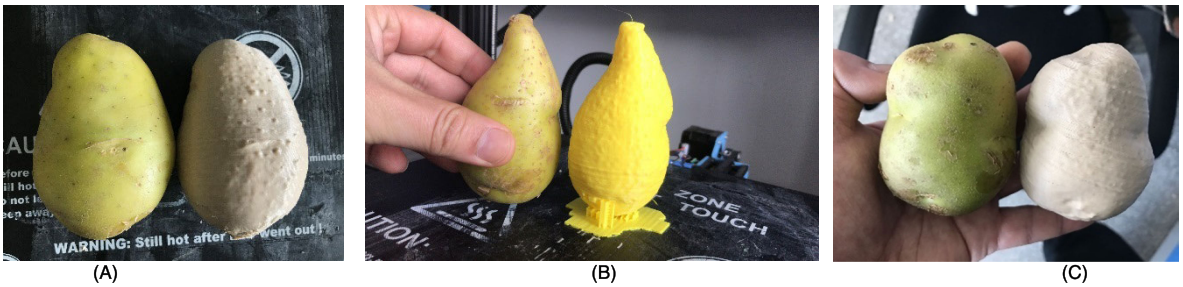

FIGURE 11. Real potatoes and 3D printed potatoes.

point cloud is −0.4%, the average relative error after interpolation is 0.29%, and the average relative error after smoothing is −0.08%. In addition, the volume of the potato in Fig. 10 was studied using 3D point cloud repair, after which the measurement error could be reduced by 1.14%. This means that point cloud repair has a small impact on the measurement of volume, but a large impact on 3D visualization. By changing the potato's volume, we can see that our processing methods are beneficial and useful in correcting the volume of the potato.

The relative error between the measured volume and estimated mass of potatoes is shown in Fig. 13.

The average relative error of potato volume in the verification group is −0.08%, the maximum relative error is 2.17%, and the minimum relative error is 0.03%. The volume, mass, and surface point cloud of the potato can be obtained simultaneously with structured light and camera. The volume of the potato can be accurately measured, and a fixed density can be used to estimate its mass. The average relative error of the estimated mass is 0.48%, and the maximum and minimum relative errors are 2.92% and 0.12%, respectively. In comparison, the average error of cauliflower volume measured by Kinect was 0.58% [29], the average error of grape volume measured by air displacement techniques was 3.8% [51], and the average error of potato volume measured by RGB-D camera was 9% [52]. Our device has obvious advantages in accuracy, at a much lower cost.

The linear correlation equation between the measured and standard volume of potatoes was analyzed using SPSS. The R^2 value was found to be 1.000 with an RMSE of 1.80 cm^3; thus the measured surface volume was in good agreement with the actual volume. It is believed that the point cloud

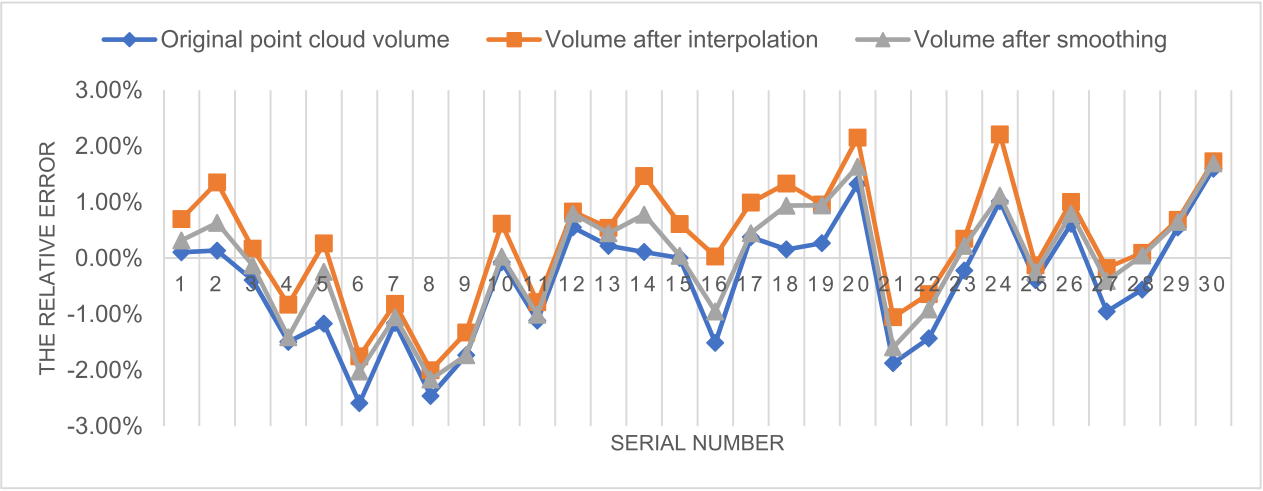

FIGURE 12. Relative error of potato volume during point cloud processing.

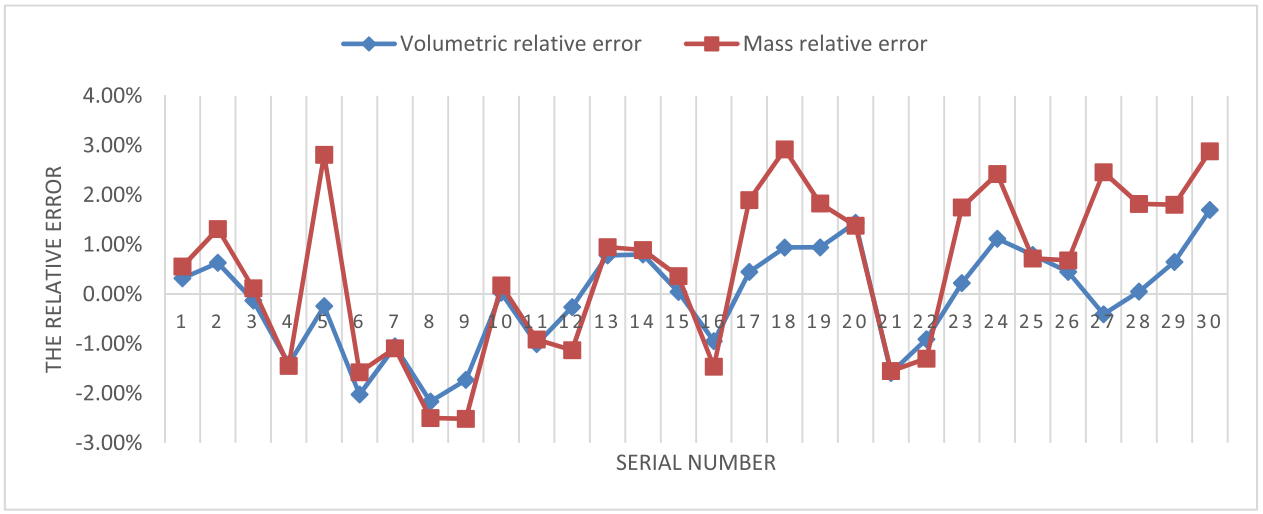

FIGURE 13. Relative error of measuring volume and estimating mass of potatoes.

coordinates obtained with the device for this paper and the reconstructed 3D model are strongly correlated with the potato surface, whose pits and buds can be visualized.

V. CONCLUSION

In this paper, a monocular camera and line laser were used to build a rotary phenotype scanning mechanism, which can be used to acquire point cloud data from the surface of a potato. We searched the point closest to the Z-axis and the intersection with the Z-axis through the point cloud at the angle of the nearest point and completed the repair of the point cloud through the intersection point and the original point cloud. Then the potatoes were sliced along the Z-axis, and the points in each section were fit to B-spline curves. The entire point cloud was used to calculate the volume and mass of a calibrated potato. The standard volume and mass of a calibrated potato were measured manually. A linear relationship between the measured and standard volume was determined using linear regression, and the density of the potato was obtained by manually measuring the mass and volume of potatoes in a modified group. The regression model of volume was used for potato verification, and the volume and mass of the potato obtained using the point cloud were compared with those that were manually measured. The coefficient of determination between potato mass and volume was 1.000, with an average relative error of −0.08% and RMSE of 1.80 cm^3. The potato mass could be accurately estimated with an average relative error of 0.48%. The results show that the error in potato mass estimation is very small. According to the NY/T 1066-2006 standard, the grading error rate of a potato is 0%. This result showed better accuracy than the 91% accuracy based on color image processing [50] and the 93% accuracy based on depth image processing [18]. This device and treatment can be used for potato grading and yield estimation. The results illustrate the usefulness of 3D point cloud reconstruction for potato phenotype reconstruction.

3D reconstruction has potential use in potato yield estimation, phenotypic studies, and quality grading. In the future, we hope to improve the performance of the system and reduce the measurement time by using depth cameras or coding structured light.

VI. ACKNOWLEDGMENT

The authors gratefully acknowledge financial support provided by the Science and Technology Innovation Engineering Project of the Chinese Academy of Agricultural Sciences under Grant CAAS office (2014) no. 216 and the Key R&D Project of Shandong Province under Grant 2019JZZY010734.

REFERENCES

[1] S. Arslan and T. S. Colvin, "Grain yield mapping: Yield sensing, yield reconstruction, and errors," *Precis. Agricult.*, vol. 3, no. 2, pp. 135–154, 2002, doi: 10.1023/A:1013819502827.

[2] P. D. C. Sanchez, N. Hashim, R. Shamsudin, and M. Z. Mohd Nor, "Applications of imaging and spectroscopy techniques for non-destructive quality evaluation of potatoes and sweet potatoes: A review," *Trends Food Sci. Technol.*, vol. 96, pp. 208–221, Feb. 2020, doi: 10.1016/j.tifs.2019.12.027.

[3] J. Gené-Mola, E. Gregorio, F. Auat Cheein, J. Guevara, J. Llorens, R. Sanz-Cortiella, A. Escolá, and J. R. Rosell-Polo, "Fruit detection, yield prediction and canopy geometric characterization using LiDAR with forced air flow," *Comput. Electron. Agricult.*, vol. 168, Jan. 2020, Art. no. 105121, doi: 10.1016/j.compag.2019.105121.

[4] J. Mack, C. Lenz, J. Teutrine, and V. Steinhage, "High-precision 3D detection and reconstruction of grapes from laser range data for efficient phenotyping based on supervised learning," *Comput. Electron. Agricult.*, vol. 135, pp. 300–311, Apr. 2017, doi: 10.1016/j.compag.2017.02.017.

[5] Y. Wang and Y. Chen, "Fruit morphological measurement based on three-dimensional reconstruction," *Agronomy*, vol. 10, no. 4, p. 455, Mar. 2020, doi: 10.3390/agronomy10040455.

[6] R. T. Furbank and M. Tester, "Phenomics–technologies to relieve the phenotyping bottleneck," *Trends Plant Sci.*, vol. 16, no. 12, pp. 635–644, Dec. 2011, doi: 10.1016/j.tplants.2011.09.005.

[7] A. Paproki, X. Sirault, S. Berry, R. Furbank, and J. Fripp, "A novel mesh processing based technique for 3D plant analysis," *BMC Plant Biol.*, vol. 12, no. 1, p. 63, 2012, doi: 10.1186/1471-2229-12-63.

[8] C. N. Topp, A. S. Iyer-Pascuzzi, J. T. Anderson, C.-R. Lee, P. R. Zurek, O. Symonova, Y. Zheng, A. Bucksch, Y. Mileyko, T. Galkovskyi, B. T. Moore, J. Harer, H. Edelsbrunner, T. Mitchell-Olds, J. S. Weitz, and P. N. Benfey, "3D phenotyping and quantitative trait locus mapping identify core regions of the rice genome controlling root architecture," *Proc. Nat. Acad. Sci. USA*, vol. 110, no. 18, pp. E1695–E1704, Apr. 2013, doi: 10.1073/pnas.1304354110.

[9] B. Li, H. M. Cockerton, A. W. Johnson, A. Karlström, E. Stavridou, G. Deakin, and R. J. Harrison, "Defining strawberry uniformity using 3D imaging and genetic mapping," *bioRxiv*, 2020, 10.1101/2020.03.01.972190.

[10] Y. Hu, L. Wang, L. Xiang, Q. Wu, and H. Jiang, "Automatic non-destructive growth measurement of leafy vegetables based on kinect," *Sensors*, vol. 18, no. 3, p. 806, Mar. 2018, doi: 10.3390/s18030806.

[11] G. P. Moreda, J. Ortiz-Cañavate, F. J. García-Ramos, and M. Ruiz-Altisent, "Non-destructive technologies for fruit and vegetable size determination—A review," *J. Food Eng.*, vol. 92, no. 2, pp. 119–136, May 2009, doi: 10.1016/j.jfoodeng.2008.11.004.

[12] G. ElMasry, S. Cubero, E. Moltó, and J. Blasco, "In-line sorting of irregular potatoes by using automated computer-based machine vision system," *J. Food Eng.*, vol. 112, nos. 1–2, pp. 60–68, Sep. 2012, doi: 10.1016/j.jfoodeng.2012.03.027.

[13] A. Dacal-Nieto, E. Vazquez-Fernandez, A. Formella, F. Martin, S. Torres-Guijarro, and H. Gonzalez-Jorge, "A genetic algorithm approach for feature selection in potatoes classification by computer vision," in *Proc. 35th Annu. Conf. IEEE Ind. Electron.*, Porto, Portugal, Nov. 2009, pp. 1955–1960, doi: 10.1109/IECON.2009.5414871.

[14] K. Vijayarekha, "Machine vision application for food quality: A review," *Res. J. Appl. Sci. Eng. Technol.*, vol. 4, pp. 5453–5458, Dec. 2012.

[15] A. M. Rady and D. E. Guyer, "Rapid and/or nondestructive quality evaluation methods for potatoes: A review," *Comput. Electron. Agricult.*, vol. 117, pp. 31–48, Sep. 2015, doi: 10.1016/j.compag.2015.07.002.

[16] J. Torppa, J. P. T. Valkonen, and K. Muinonen, "Three-dimensional stochastic shape modelling for potato tubers," *Potato Res.*, vol. 49, no. 2, pp. 109–118, Jan. 2007, doi: 10.1007/s11540-006-9010-5.

[17] B. Li, X. Xu, L. Zhang, J. Han, C. Bian, G. Li, J. Liu, and L. Jin, "Above-ground biomass estimation and yield prediction in potato by using UAV-based RGB and hyperspectral imaging," *ISPRS J. Photogramm. Remote Sens.*, vol. 162, pp. 161–172, Apr. 2020, doi: 10.1016/j.isprsjprs.2020.02.013.

[18] Q. Su, N. Kondo, M. Li, H. Sun, and D. F. Al Riza, "Potato feature prediction based on machine vision and 3D model rebuilding," *Comput. Electron. Agricult.*, vol. 137, pp. 41–51, May 2017, doi: 10.1016/j.compag.2017.03.020.

[19] T. Palleja, M. Tresanchez, M. Teixido, R. Sanz, J. R. Rosell, and J. Palacin, "Sensitivity of tree volume measurement to trajectory errors from a terrestrial LIDAR scanner," *Agricult. Forest Meteorol.*, vol. 150, no. 11, pp. 1420–1427, Oct. 2010, doi: 10.1016/j.agrformet.2010.07.005.

[20] E. González-Ferreiro, U. Diéguez-Aranda, and D. Miranda, "Estimation of stand variables in pinus radiata D. Don plantations using different LiDAR pulse densities," *Forestry, Int. J. Forest Res.*, vol. 85, no. 2, pp. 281–292, Apr. 2012, doi: 10.1093/forestry/cps002.

[21] A. F. Colaço, R. G. Trevisan, J. P. Molin, and J. R. Rosell-Polo, "Spatial variability of canopy volume in a commercial citrus grove" presented at the 13th Int. Conf. Precis. Agricult., Int. Society of Precis. Agricult., St. Louis, MI, USA, 2016.

[22] M. Hämmerle and B. Höfle, "Effects of reduced terrestrial LiDAR point density on high-resolution grain crop surface models in precision agriculture," *Sensors*, vol. 14, no. 12, pp. 24212–24230, Dec. 2014, doi: 10.3390/s141224212.

[23] F. P. Boogaard, K. S. A. H. Rongen, and G. W. Kootstra, "Robust node detection and tracking in fruit-vegetable crops using deep learning and multi-view imaging," *Biosystems Eng.*, vol. 192, pp. 117–132, Apr. 2020, doi: 10.1016/j.biosystemseng.2020.01.023.

[24] P. Negretti, G. Bianconi, and A. Finzi, "Visual image analysis to estimate morphological and weight measurements in rabbits," *World Rabbit Sci.*, vol. 15, no. 1, pp. 37–41, Jul. 2010, doi: 10.4995/wrs.2007.606.

[25] K. Kawasue, K. D. Win, K. Yoshida, and T. Tokunaga, "Black cattle body shape and temperature measurement using thermography and KINECT sensor," *Artif. Life Robot.*, vol. 22, no. 4, pp. 464–470, Jun. 2017, doi: 10.1007/s10015-017-0373-2.

[26] P. Menesatti, C. Costa, F. Antonucci, R. Steri, F. Pallottino, and G. Catillo, "A low-cost stereovision system to estimate size and weight of live sheep," *Comput. Electron. Agricult.*, vol. 103, pp. 33–38, Apr. 2014, doi: 10.1016/j.compag.2014.01.018.

[27] A. K. Mortensen, A. Bender, B. Whelan, M. M. Barbour, S. Sukkarieh, H. Karstoft, and R. Gislum, "Segmentation of lettuce in coloured 3D point clouds for fresh weight estimation," *Comput. Electron. Agricult.*, vol. 154, pp. 373–381, Nov. 2018, doi: 10.1016/j.compag.2018.09.010.

[28] W. Wang and C. Li, "Size estimation of sweet onions using consumer-grade RGB-depth sensor," *J. Food Eng.*, vol. 142, pp. 153–162, Dec. 2014, doi: 10.1016/j.jfoodeng.2014.06.019.

[29] D. Andújar, A. Ribeiro, C. Fernández-Quintanilla, and J. Dorado, "Using depth cameras to extract structural parameters to assess the growth state and yield of cauliflower crops," *Comput. Electron. Agricult.*, vol. 122, pp. 67–73, Mar. 2016, doi: 10.1016/j.compag.2016.01.018.

[30] M. J. Lerma-García, C. Lantano, E. Chiavaro, L. Cerretani, J. M. Herrero-Martínez, and E. F. Simó-Alfonso, "Classification of extra virgin olive oils according to their geographical origin using phenolic compound profiles obtained by capillary electrochromatography," *Food Res. Int.*, vol. 42, no. 10, pp. 1446–1452, Dec. 2009, doi: 10.1016/j.foodres.2009.07.027.

[31] A. Gongal, S. Amatya, M. Karkee, Q. Zhang, and K. Lewis, "Sensors and systems for fruit detection and localization: A review," *Comput. Electron. Agricult.*, vol. 116, pp. 8–19, Aug. 2015, doi: 10.1016/j.compag.2015.05.021.

[32] J. Gené-Mola, V. Vilaplana, J. R. Rosell-Polo, J.-R. Morros, J. Ruiz-Hidalgo, and E. Gregorio, "Multi-modal deep learning for fuji apple detection using RGB-D cameras and their radiometric capabilities," *Comput. Electron. Agricult.*, vol. 162, pp. 689–698, Jul. 2019, doi: 10.1016/j.compag.2019.05.016.

[33] J. Tamás, P. Riczu, G. Nagy, A. Nagy, T. Jancsó, J. Nyéki, and Z. Szabó, "Applicability of 3D laser scanning in precision horticulture," *Int. J. Horticultural Sci.*, vol. 17, nos. 4–5, pp. 55–58, Dec. 2011.

[34] T. Chalidabhongse, P. Yimyam, and P. Sirisomboon, "2D/3D vision-based Mango's feature extraction and sorting," in *Proc. 9th Int. Conf. Control, Autom., Robot. Vis.*, Singapore, Dec. 2006, pp. 1–6, doi: 10.1109/ICARCV.2006.345248.

[35] J. Rose, S. Paulus, and H. Kuhlmann, "Accuracy analysis of a multi-view stereo approach for phenotyping of tomato plants at the organ level," *Sensors*, vol. 15, no. 5, pp. 9651–9665, Apr. 2015, doi: 10.3390/s150509651.

[36] F. Golbach, G. Kootstra, S. Damjanovic, G. Otten, and R. van de Zedde, "Validation of plant part measurements using a 3D reconstruction method suitable for high-throughput seedling phenotyping," *Mach. Vis. Appl.*, vol. 27, no. 5, pp. 663–680, Jul. 2016, doi: 10.1007/s00138-015-0727-5.
[37] M. J. Westoby, J. Brasington, N. F. Glasser, M. J. Hambrey, and J. M. Reynolds, "'Structure-from-Motion' photogrammetry: A low-cost, effective tool for geoscience applications," *Geomorphology*, vol. 179, pp. 303–314, Dec. 2012, doi: 10.1016/j.geomorph.2012.08.021.
[38] M. A. Fonstad, J. T. Dietrich, B. C. Courville, J. L. Jensen, and P. E. Carbonneau, "Topographic structure from motion: A new development in photogrammetric measurement," *Earth Surf. Processes Landforms*, vol. 38, no. 4, pp. 421–430, Mar. 2013, doi: 10.1002/esp.3366.
[39] S. Yamamoto, M. Karkee, Y. Kobayashi, N. Nakayama, S. Tsubota, L. N. T. Thanh, and T. Konya, "3D reconstruction of apple fruits using consumer-grade RGB-depth sensor," *Eng. Agricult., Environ. Food*, vol. 11, no. 4, pp. 159–168, Oct. 2018, doi: 10.1016/j.eaef.2018.02.005.
[40] S. R. Aylward and E. Bullitt, "Initialization, noise, singularities, and scale in height ridge traversal for tubular object centerline extraction," *IEEE Trans. Med. Imag.*, vol. 21, no. 2, pp. 61–75, 2002, doi: 10.1109/42.993126.
[41] M. S. Hassouna and A. A. Farag, "Robust centerline extraction framework using level sets," in *Proc. IEEE Comput. Soc. Conf. Comput. Vis. Pattern Recognit. (CVPR)*, San Diego, CA, USA, Jun. 2005, pp. 458–465, doi: 10.1109/CVPR.2005.306.
[42] J. C. Carr, R. K. Beatson, J. B. Cherrie, T. J. Mitchell, W. R. Fright, B. C. McCallum, and T. R. Evans, "Reconstruction and representation of 3D objects with radial basis functions," in *Proc. 28th Annu. Conf. Comput. Graph. Interact. Techn. (SIGGRAPH)*, Los Angeles, CA, USA, 2001, pp. 67–76, doi: 10.1145/383259.383266.
[43] C. Xiao, W. Zheng, Y. Miao, Y. Zhao, and Q. Peng, "A unified method for appearance and geometry completion of point set surfaces," *Vis. Comput.*, vol. 23, no. 6, pp. 433–443, May 2007, doi: 10.1007/s00371-007-0115-x.
[44] S. Park, X. Guo, H. Shin, and H. Qin, "Shape and appearance repair for incomplete point surfaces," in *Proc. 10th IEEE Int. Conf. Comput. Vis. (ICCV)*, vol. 1, Beijing, China, Jun. 2005, pp. 1260–1267, doi: 10.1109/ICCV.2005.218.
[45] N. N. Cuong, K. Veroy, and A. T. Patera, "Certified real-time solution of parametrized partial differential equations," in *Handbook of Materials Modeling*, S. Yip, Eds. Dordrecht, The Netherlands: Springer, 2005, pp. 1529–1564, doi: 10.1007/978-1-4020-3286-8_76.
[46] G. E. Farin and G. Farin, Eds., *Curves and Surfaces for CAGD: A Practical Guide*. Burlington, MA, USA: Morgan Kaufmann, 2002.
[47] F. Bernardini, J. Mittleman, H. Rushmeier, C. Silva, and G. Taubin, "The ball-pivoting algorithm for surface reconstruction," *IEEE Trans. Vis. Comput. Graphics*, vol. 5, no. 4, pp. 349–359, Oct. 1999, doi: 10.1109/2945.817351.
[48] F. Liu, Y. Zhuang, F. Wu, and Y. Pan, "3D motion retrieval with motion index tree," *Comput. Vis. Image Understand.*, vol. 92, nos. 2–3, pp. 265–284, Nov. 2003, doi: 10.1016/j.cviu.2003.06.001.
[49] S. Krishnan, P. Y. Lee, J. B. Moore, and S. Venkatasubramanian, "Global registration of multiple 3D point sets via optimization on a manifold," U.S. Patent 7 831 090 B1, Nov. 9, 2010.
[50] Z. Zhou, Y. Huang, X. Li, D. Wen, C. Wang, and H. Tao, "Automatic detecting and grading method of potatoes based on machine vision," *Trans. Chin. Soc. Agricult. Eng.*, vol. 28, no. 7, pp. 178–183, 2012.
[51] V. Iraguen, A. Guesalaga, and E. Agosin, "A portable non-destructive volume meter for wine grape clusters," *Meas. Sci. Technol.*, vol. 17, no. 12, pp. N92–N96, Dec. 2006.
[52] Y. Long, Y. Wang, Z. Zhai, L. Wu, M. Li, H. Sun, and Q. Su, "Potato volume measurement based on RGB-D camera," *IFAC-PapersOnLine*, vol. 51, no. 17, pp. 515–520, 2018.

ZEYU CAI received the B.Sc. degree in thermal and power engineering from Northwestern Polytechnical University, Xi'an, China, in 2014. He is currently pursuing the M.Sc. degree in agricultural mechanization engineering with the Chinese Academy of Agricultural Sciences, Beijing, China. His research interests include point cloud processing and machine vision.

CHENGQIAN JIN received the B.Sc. degree in agricultural mechanization engineering from Huazhong Agricultural University, Hubei, China, in 1995, the M.Sc. degree in agricultural mechanization engineering from the Nanjing University of Science and Technology, Nanjing, China, in 2006, and the Ph.D. degree in agricultural mechanization engineering from Nanjing Agricultural University, Nanjing, in 2014. He is currently a Researcher with the Chinese Academy of Agricultural Sciences and a Professor with the Shandong University of Technology. His major is in agricultural mechanization engineering.

JING XU received the B.Sc. degree in instrumentation engineering from the Nanjing University of Science and Technology, Nanjing, China, in 2015. She is currently a Metrologist with the Jiangsu Institute of Metrology. Her research interest includes mechanical measurement.

TENGXIANG YANG received the B.Sc. degree in agricultural mechanization engineering from the Shandong University of Technology, China, in 2017, and the M.Sc. degree in agricultural mechanization engineering from the Chinese Academy of Agricultural Sciences, Beijing, China. He is currently a Researcher with the Chinese Academy of Agricultural Sciences. His research interests include automatic control and automation.